Icarus **147**, 433–443 (2000)
doi:10.1006/icar.2000.6459, available online at http://www.idealibrary.com on IDEAL®

Topography and Stratigraphy of the Northern Martian Polar Layered Deposits Using Photoclinometry, Stereogrammetry, and MOLA Altimetry

Lori K. Fenton

Division of Geological and Planetary Sciences, California Institute of Technology, Pasadena, California 91125
E-mail: lori@gps.caltech.edu

and

Ken E. Herkenhoff

Astrogeology Team, United States Geological Survey, Flagstaff, Arizona 86001

Received January 3, 2000; revised May 25, 2000

We present two photoclinometric profiles across a trough in the martian northern polar layered terrain. Complications caused by albedo variations were avoided by using an early springtime *Viking* image with a thin cover of seasonal CO_2 frost. The topographic profiles were constrained with stereogrammetric elevations derived from summertime *Viking* images of the same region.

We find that the photoclinometric profiles are consistent with a nearby MOLA (Mars Orbiter Laser Altimeter) track crossing the same polar trough. The trough is asymmetric, with higher relief and a steeper slope on the equatorward-facing wall. Individual layers are subdued and difficult to observe in the profiles. A decrease in both relief and elevation toward the eastern end of the trough suggests that layers become thinner to the east. Declining equatorward slopes in the eastern portion of the trough imply that erosion rates have varied along the trough. The variation in erosion rate may be linked to the change in layer thickness along the trough.

Layers have an average thickness of 19 ± 8 m in the center of the trough and 59 ± 32 m on the northern wall. The northern wall is most likely composed of thinner layers that are obscured. To first order, we find that a 19-m layer requires 16,000 years of deposition to form. Although this timescale does not coincide with orbital variation periods of 10^5 and 10^6 years, deposition rates may not be constant and thus the 16,000-year layer formation time does not preclude layer formation during part of each orbital oscillation.

Key Words: **Mars; Mars, surface; Mars, climate; surfaces, planets.**

1. INTRODUCTION

The martian polar layered deposits have long been regarded as a geologic record of sedimentary deposition. It is widely believed that the polar layered deposits record climate variations over the past 10 to 100 million years (Murray *et al.* 1972; Cutts *et al.* 1976, 1979; Squyres 1979; Toon *et al.* 1980; Carr 1982; Howard *et al.* 1982a; Plaut *et al.* 1988), but the details of the processes involved remain obscure (Thomas *et al.* 1992). Variations in axial obliquity, orbital eccentricity, and precession are thought to influence the climates of both Earth and Mars, but are of greater amplitude for Mars (Ward 1974, 1979; Bills 1990). A common presumption among Mars researchers is that the layered deposits are the result of variations in the proportions of dust and water ice deposited over many climate cycles (Cutts *et al.* 1979, Squyres 1979, Toon *et al.* 1980).

In this work a single layer is defined as a dark and light stripe "pair." Thus each pair corresponds to a single "step" in which one stripe corresponds to a relatively horizontal surface and the other stripe corresponds to a relatively steeper surface. Layers are exposed in ∼10-km-wide troughs in both polar regions of Mars. These troughs spiral away from the pole and cut through the residual ice caps. The layered deposits are similar in color and albedo to martian dust, much darker than the polar ice (Thomas and Weitz 1989, Herkenhoff and Murray 1990a). The detailed composition of these layers is poorly constrained (Malin 1986), but it is commonly assumed to be a mixture of dust and water ice. These layers have similar thicknesses that extend with parallel contacts and little observable deformation for hundreds of kilometers along the trough walls and presumably beneath the permanent ice cap as well. Howard *et al.* (1982b) found angular unconformities in the north polar layered deposits, but not in the south.

Individual layers can be traced for large distances along trough walls (Malin and Edgett 1999), but their extent beneath the overlying residual ice is not known. Layers exposed in a trough on one side of the polar cap may extend to the other side of the polar cap. If this is the case then each layer must have been deposited across the entire polar region at roughly the

0019-1035/00 $35.00

same rate. Alternatively, layers may have been deposited over smaller areas, indicating local rather than regional deposition (Howard *et al.* 1982a). Thus there is a strong need for measurements of the stratigraphic sequence of layers in each trough in order to determine the history of the layered deposits. Slight differences in thickness from layer to layer appear to be characteristic of the layered deposits. Measurement of layer thickness sequences may be the best way to correlate layers exposed in different troughs. The main purpose of this research is to demonstrate a technique that creates accurate topographic profiles, determines the detailed stratigraphy of the layered deposits, and forms a trough-wide context for future studies.

Several researchers have used photoclinometric topographic profiles, in some cases combined with stereogrammetric elevations, to determine the topography across polar troughs (Blasius *et al.* 1982a, Herkenhoff and Murray 1990b). In this work we present two photoclinometric profiles across a trough in the northern polar layered terrain. Because photoclinometric methods often produce nonunique topographic profiles, we constrained the profiles with stereogrammetric elevations.

The data from the Mars Global Surveyor will produce new information with regard to the martian polar layered terrain. Mars Orbital Camera (MOC) imagery adds detail to the lower resolution images of the *Viking Orbiters* (Malin and Edgett 1999). The contextual information provided by *Viking* images has proven useful in interpreting new MOC images (e.g., Chapman 1999). The Mars Orbiter Laser Altimeter (MOLA) provides accurate profiles, absolute elevations, and locations better than that derived from *Viking* data. However, MOLA profiles are limited to the roughly 300-m horizontal spacing of about 160-m-wide footprints (Zuber *et al.* 1992). Photoclinometry creates topographic profiles at the resolution of the image used. Therefore photoclinometry is still a useful tool, especially if constrained by MOLA elevations. In this work we compare photoclinometrically determined profiles with MOLA profiles.

2. DATA AND METHOD

2.1. Overview and Image Selection

The method used here combines photoclinometry with stereogrammetry. Photoclinometry uses differences in reflected sunlight as an indicator of change in slope. Slopes can then be integrated to create a two-dimensional topographic profile. Unfortunately the observed intensity is a function of both slope and surface albedo, with these two effects usually inseparable. The simplest way of attacking this problem is to assume that the surface has a constant albedo. This assumption is reasonable in the polar regions when a CO_2 frost 0.5–1.0 m thick (Paige and Ingersoll 1985) is present during the winter and early spring. We assume that this frost obscures any underlying albedo features. We chose an image (499B46) centered at 83.65°N, 306.25°W that was taken during the early northern spring at $L_s = 26.51°$ (shown in Fig. 1a). Every feature in Fig. 1a is assumed to be visible due to shading from changes in slope. The prominent linear feature in the image is one of the erosional troughs in the polar cap that exposes several layers. This particular trough is 15 km wide and includes an elongated ridge bisecting its center that is hereafter referred to as the "midridge."

Stereogrammetry uses differences in the viewing angle of two images, or parallax, to determine distance from the spacecraft and thus surface elevation. A stereo pair of summertime images (77B25, $L_s = 144.58°$ and 77B55, $L_s = 144.59°$) of the area in Fig. 1a was found, one of which is shown in Fig. 1b. A study of *Viking* images showed that this is one of the very few areas where both summer stereo coverage and a springtime image are available. Because they show more surface features and are at higher resolution, the summertime images are more useful for stereogrammetry than springtime images.

During the summer the seasonal CO_2 frost sublimates, revealing the dark layers in the trough, which is incised into the surrounding bright permanent ice cap. Note that there is a prominent layer in the northern wall (see arrows, Fig. 1) that is dark in the springtime image and bright in the summertime image. This intensity reversal has been verified by careful distance measurements and comparison between the spring and summertime images. Other less distinct layers also show this seasonal reversal. This change in apparent brightness can be explained by the effects of slope. In the winter and spring when the seasonal CO_2 cap obscures any albedo features, a level surface would receive less insolation than a surface facing the Sun (south, in this case). Thus less light would be reflected to the spacecraft from a level surface than from a surface facing the Sun, and this prominent dark line must be a relatively level surface. During the summer, slopes facing the Sun would undergo more sublimation revealing the underlying dark material. Level surfaces would undergo less sublimation, possibly becoming centers of local frost accumulation. Thus the level surfaces that appear relatively darker during the spring could appear relatively brighter during the summer due to frost retention.

2.2. Stereogrammetry

Twenty-one stereogrammetric elevations were found in the trough using a digital routine developed for the USGS Planetary Image Cartography System (PICS) (Edwards 1987, Batson 1987). Each elevation found required manual identification of a single small feature in both summertime images. Unfortunately few places in the images were distinct enough to identify on both images in the trough, and none at all were found on the bright permanent ice cap.

Figure 2 shows the stereogrammetric elevations and locations mapped onto the springtime image. The elevations are shown relative to a reference planetary radius of 3375 km. Because of uncertainties in feature locations the elevation errors are often quite large.

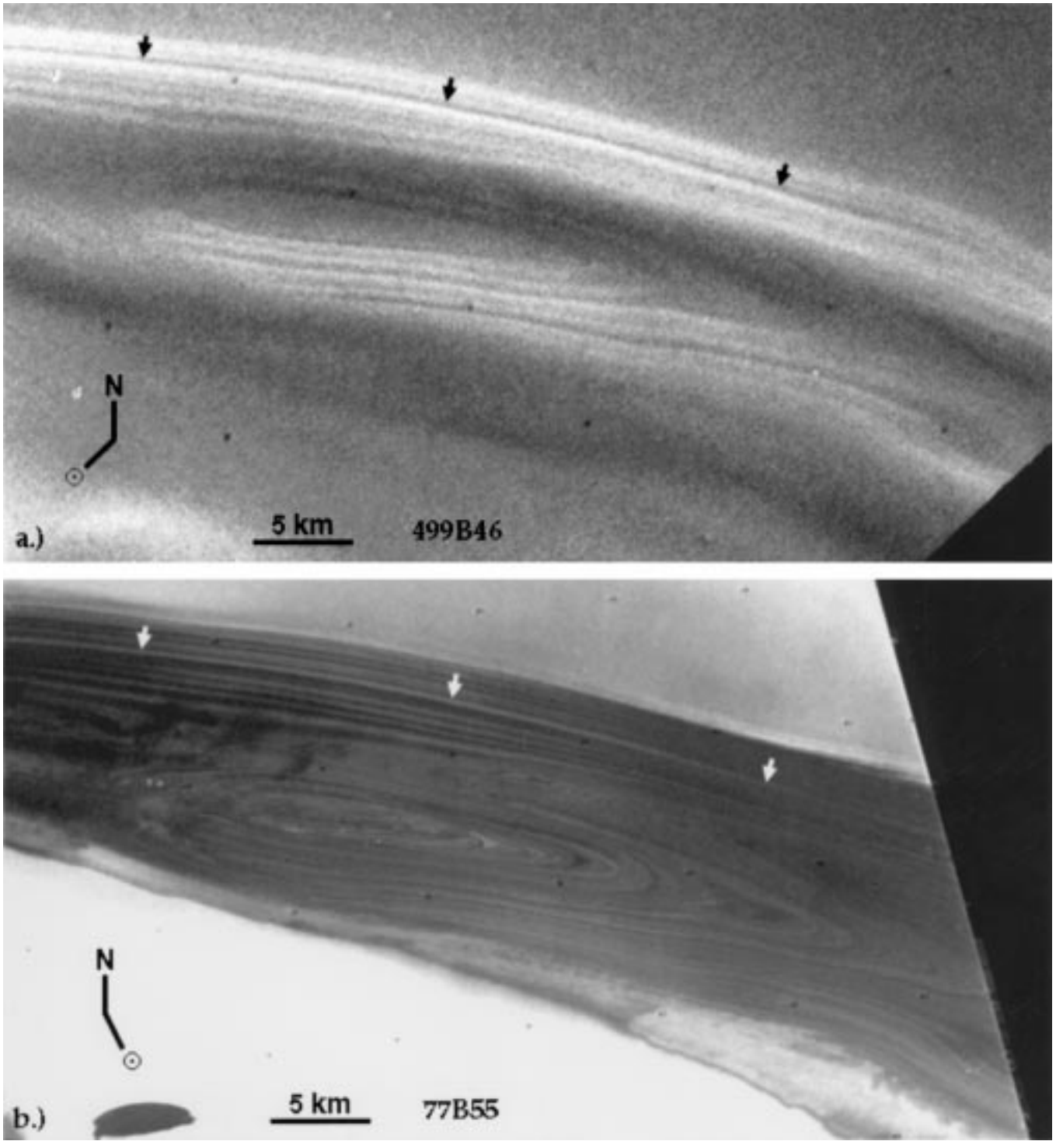

FIG. 1. (a) *Viking* springtime image (499B46) of the polar trough, covered in CO_2 frost ($L_s = 26.51^\circ$, 70 m/pix). Directions toward north and the Sun are indicated. Arrows point to a prominent layer that reverses intensity in the summer. (b) Summertime image (077B55) of the same trough, after CO_2 has sublimated away ($L_s = 144.59^\circ$, 50 m/pix but shown here at 70 m/pix for comparison with 499B46). Directions toward north and the Sun are indicated. Note change in intensity of layer (see arrows).

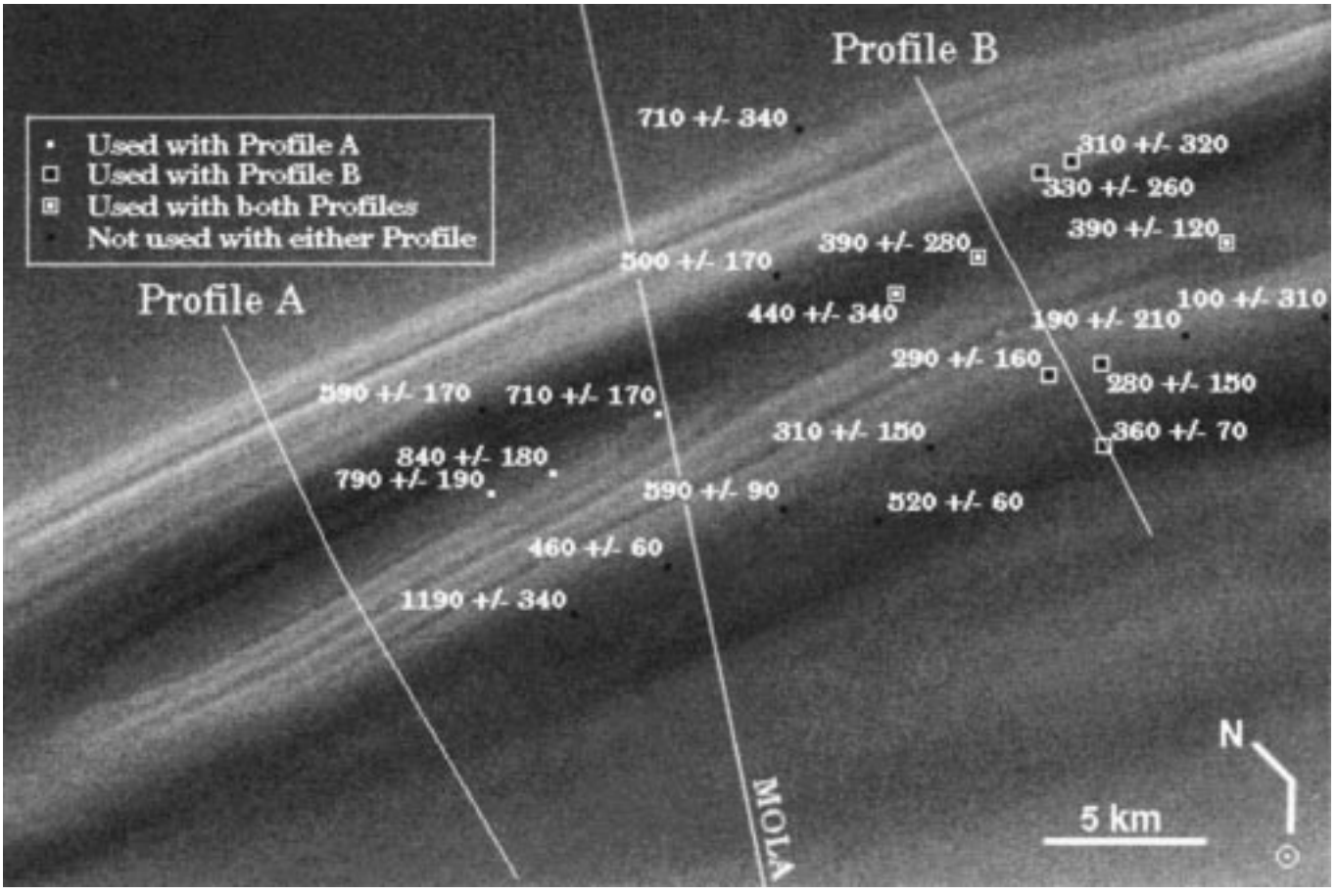

FIG. 2. *Viking* image 499B46 showing the location of photoclinometric profiles A and B, all 22 stereogrammetric elevations, and the MOLA profile. Directions toward north and the Sun are indicated.

Figure 2 also shows which stereogrammetric points correspond to each photoclinometric profile. These points were chosen either because they were located close to their respective profile lines or because they fell on layers that cross profile lines. In this work we have assumed that the trough layers are approximately level (described below in Section 2.5), so each stereogrammetric elevation that falls on a layer determines the elevation of the entire layer. Thus we were able to include stereogrammetric points far from the actual location of the profile (for example, 390 ± 120 m falls on a layer crossing both profiles). Unused stereogrammetric points in Fig. 2 are still valid but they were not used in this study because they are located too far from the profiles and they do not occur on identifiable layers.

The stereogrammetric points used to constrain each photoclinometric profile are listed in Table I. If two stereogrammetric points were located on the same layer (for example, 790 ± 190 and 840 ± 180 m) then we used the weighted average and the weighted average error. If two points fell near the profile line but not on any observable layer (for example, 330 ± 260 and 310 ± 320 m) then we again used the weighted average and weighted average error.

2.3. Photoclinometry

We use the same method of calculating photoclinometric profiles used by Howard *et al.* (1982b). We have assumed that a Lambertian surface can be applied to the seasonal CO_2 frost in the north polar regions. The intensity of each image pixel represents a combination of light reflected from the surface and light scattered by atmospheric aerosols. Here we assume that the atmospheric component can be approximated by a simple constant

TABLE I
Stereo Points Used for Each Profile

Profile A		Profile B	
Elevation	Comment	Elevation	Comment
710 ± 170	On connecting layer	322 ± 202	Avg. nearby points
816 ± 131	Avg. pts on layer	410 ± 216	Avg. pts on layer
816 ± 131	Avg. pts on layer	410 ± 216	Avg. pts on layer
710 ± 170	On connecting layer	390 ± 120	On connecting layer
410 ± 216	Avg. pts on layer	290 ± 160	Close to profile line
390 ± 120	On connecting layer	280 ± 150	Close to profile line
		360 ± 70	On profile line

that affects each pixel equally. Using these approximations and the theory developed in Howard *et al.* (1982) we arrive at the relation

$$\frac{\frac{I}{F}_{\text{meas}} - \frac{I}{F}_{\text{atm}}}{\frac{I}{F}_{\text{horiz}} - \frac{I}{F}_{\text{atm}}} = \cos\theta - \tan i \sin\theta \sin\psi, \qquad (1)$$

where $\frac{I}{F}_{\text{meas}}$ is the measured reflected intensity (I) relative to the incident sunlight (F), $\frac{I}{F}_{\text{horiz}}$ is the $\frac{I}{F}_{\text{meas}}$ for a horizontal surface, $\frac{I}{F}_{\text{atm}}$ is the reflected intensity of atmospheric particles relative to the incident sunlight, θ is the slope of the surface, i is the solar incidence angle, and ψ is the angle between the solar azimuth and the strike of the slope being measured. We assume that i and ψ remain constant along each profile. The slope angle, θ, is the parameter we solved for.

Equation (1) is transcendental and thus the slope θ cannot be solved analytically. We created an array of possible θ values and iteratively fitted them to Eq. (1) until a "best-fit" θ was found to be within 0.002°. Profiles were then created by integrating the slope into elevation as a function of distance along the profile line.

2.4. Choosing Profiles

We chose two profile locations that cross the exposed layers in the trough, labeled Profiles A and B in Fig. 2. Profile A crosses the midridge that bisects the trough. Profile B crosses the trough at a place where the midridge is very subdued. Both profiles were aligned normally to the exposed layers not only to achieve the best estimate of the true layer and hill slopes, but also to project as many points possible without smear along the profile line. If the profiles are not normal to the layers then the slope estimates will be lower than their true values.

To diminish this effect and the pixel-to-pixel noise inherent in the Visual Imaging Subsystem (VIS) system we used a wide swath of pixels along both profiles. The process of projecting pixels onto a line is well described in Howard *et al.* (1982b). Because the trough layers crossing Profile A are very straight and consistent, we chose a profile half-width of 20 pixels. For Profile B we used a half-width of 10 pixels because the trough layers are less straight than those near Profile A.

2.5. The Assumption of Level Layers

We have assumed that the layers exposed in the trough are roughly horizontal. Sedimentary materials are usually deposited in horizontal layers, remaining so unless deformed, faulted, or tilted. We can qualitatively justify that the trough layers have remained unmoved from their deposited state. Profiles A and B are roughly 20 km apart. Along both the northern wall and the southern side of the midridge, layers are exposed along the entire distance between Profiles A and B. Along this distance the layers never appear to tilt up the wall in Fig. 2. Even if the layers climb up the wall by about 10% of the height of the wall, or roughly 60 m, then the dip angle would be only 0.17°. A similar constraint can be used across the trough along Profile A where layers along the midridge wrap around the island and cross Profile A twice. If the layers again climb up the midridge by about 10% of its height, or roughly 20 m, then the dip angle again would be only 0.17°. These dip constraints in two perpendicular directions limit the overall dip of the layers in any direction.

We have assumed that the cliff at the top of the trough is roughly horizontal. This assumption is not sensitive to the case in which the trough cliff and its layers both tilt in the same direction.

The assumption of level layers has been necessary in this work and it has been used in several ways. It is first used to determine $\frac{I}{F}_{\text{horiz}}$, for fitting the two profiles to stereogrammetric elevations, and finally for tying the two profiles together. We have noted each case where the assumption was made.

2.6. Image Calibration

Before finding photoclinometic profiles on the springtime image we calibrated the image using standard routines from the PICS. However there is one problem that PICS does not correct.

The vidicons of the *Viking Orbiter* cameras (VIS) generated dark current with variable amplitude across the image frame (E. Eliason, personal communication, 1999). This dark current "ramp" is not always fully corrected by the PICS calibration routines, but can be measured in the two dark masks at either edge of the vidicon. When properly calibrated, the intensity in these two dark strips should be zero. If the dark ramp is not corrected then both absolute and relative radiometric measurements of the *Viking* image may be in error. We measured the intensity along each dark strip and interpolated across the image, assuming that the variation across the image is linear. The variation may not be linear, but no better correction is available. This interpolated ramp array was subtracted from the entire image, yeilding a first-order correction to the residual dark current.

2.7. Estimating $\frac{I}{F}_{horiz}$

Equation (1) above requires an estimate of $\frac{I}{F}_{\text{horiz}}$, the fraction of reflected sunlight from a horizontal surface. From imaging alone there is no reliable method for estimating what part of an image represents a truly horizontal surface. Howard *et al.* (1982b) assumed that there was no net slope across an entire image, and that therefore the mean $\frac{I}{F}$ of the entire image was a good estimate of $\frac{I}{F}_{\text{horiz}}$. However the springtime image 499B46 is located near the edge of the northern polar cap, and there is reason to believe that the surface slopes down toward the polar cap margin.

Several layers in the midridge cross Profile A twice. Assuming each layer is horizontal, there should be no change in elevation from one side of the midridge to the other. The parameter $\frac{I}{F}_{\text{horiz}}$ in Eq. (1) has the effect of tilting the resulting photoclinometric profiles. We adjusted $\frac{I}{F}_{\text{horiz}}$ until the layers on either side of the midridge were at the same elevation. The resulting $\frac{I}{F}_{\text{horiz}}$ was 0.1452. The mean $\frac{I}{F}$ for the entire image was 0.1476, suggesting

a slight overall sunward (southward) tilt of the surface toward the polar cap margin.

2.8. Estimating the Atmospheric Contribution $\frac{I}{F}_{atm}$

As ground-based observers have noted for years, the northern martian polar cap accumulates a dense atmospheric "polar hood" that lasts through early spring. At the time the springtime image was acquired ($L_s = 26.51^\circ$), the atmosphere is expected to have contributed substantially to the total measured intensity in each pixel. This aerosol contribution must be accounted for to produce an accurate representation of the surface topography. One way of calculating the optical depth is by measuring the brightness of shadows. Unfortunately, there are no good shadows anywhere in image 499B46, nor in any of the adjacent images from this orbit, nor in other images of the area at this time of year. Thus the atmospheric opacity remains undetermined.

The resulting topographic profiles depend strongly on atmospheric opacity, as shown by the $\frac{I}{F}_{\text{atm}}$ factor in Eq. (1) above. We used the stereogrammetric elevations to constrain the absolute elevations of the two photoclinometric profiles. Because the stereogrammetric elevations are independent of atmospheric opacity we have also used them to constrain $\frac{I}{F}_{\text{atm}}$. The resulting profiles thus are constrained to a range of slopes, elevations, and atmospheric opacities that fit within the uncertainties of the stereogrammetric elevations.

Keeping the profiles within the range or the stereogrammetric errors results in $\frac{I}{F}_{\text{atm}}$ extremes of 0.1240 and 0.1350. Note that these values are a large percentage of the $\frac{I}{F}_{\text{horiz}}$ value of 0.1452, indicating that the brightness of the springtime image is dominated by atmospheric scattering. In Fig. 1a, the springtime image has been stretched to enhance surface features.

Two profiles were created at each location, described in detail below, corresponding to the two $\frac{I}{F}_{\text{atm}}$ extremes of 0.1240 and 0.1350. Profiles with the higher atmospheric content have higher relief because a greater constant $\frac{I}{F}_{\text{atm}}$ was subtracted from the $\frac{I}{F}_{\text{meas}}$ values. Thus the small changes in $\frac{I}{F}_{\text{meas}}$ caused by topography became a larger percentage of the overall $\frac{I}{F}_{\text{meas}}$ range, effectively stretching the image. Results are summarized in Table II.

We prefer an $\frac{I}{F}_{\text{atm}}$ value toward the low end of the range. It is difficult to believe that the north wall has a relief of 2 km when the one measured stereogrammetric point on the northern wall rim (see Fig. 2) is at most about 800 m above the trough floor.

3. RESULTS

3.1. Profiles

The resulting profiles are shown in Fig. 3. The horizontal axis shows the distance from the northernmost end of each profile. The vertical axis is the elevation relative to a 3375-km radius. The triangles correspond to stereogrammetric elevations falling on trough layers that crossed the profiles. Vertical lines are the stereogrammetric uncertainties. Each profile has been shifted vertically to fit within all of its corresponding stereogrammetric elevation error bars. In a few cases a single layer with a stereogrammetric elevation wrapped around the midridge and crossed a profile twice, so the same elevations appear on each side of the midridge.

The midridge is quite evident in both Profiles A and B as a low rise in the center of the trough. However, individual layers are very difficult to discern. Mars Orbital Camera images have also shown that northern polar layers are very subtle compared to their counterparts in the south (Malin and Edgett 1999). Smooth, asymmetric troughs with subtle layers may be characteristic of the northern polar deposits while scarps with sharp layers (Herkenhoff and Murray 1990b) may be characteristic of the southern polar deposits, but such general conclusions are speculative as they are based on observations of only a few locations.

Edgett and Malin (1999) report that some of the northern polar layers are in fact ridges rather than terraces. In more recent work they describe many layers of varying slopes and textures, some of which are less than 10 m thick (Edgett and Malin 2000). It is uncertain what effect these small-scale features have on our photoclinometric study of *Viking* images. It is likely that shadows caused by rougher terrain will lead to biased slopes in our photoclinometric profiles. The shading from the large layers seen in the *Viking* images reflects the average shading of many small layers, so the small subresolution layers will have no net effect on our photoclinometric profiles. At this time no MOC images in our study region are available so the possible effects of small-scale features remain undetermined.

The trough slopes in Profile B are lower than those in Profile A. The midridge is broader and more subdued in Profile B than in Profile A, corresponding well with the midridge's appearance in Fig. 2. All of these results indicate a decreasing relief eastward (toward Profile B). Elevations in Profile B are lower than those in Profile A. This result fits well with Fig. 1b, where older lower

TABLE II
Profile Slopes and Reliefs

		North wall		North midridge		South midridge		South wall	
	$\frac{I}{F}_{\text{atm}}$	0.124	0.135	0.124	0.135	0.124	0.135	0.124	0.135
Profile A	Slope	9.1°	20°	2.5°	5.2°	3.7°	8.0°	4.3°	8.9°
	Relief	870 m	2070 m	120 m	250 m	220 m	470 m	580 m	1200 m
Profile B	Slope	5.9°	13°	1.4°	3.0°	2.0°	4.3°	3.8°	7.9°
	Relief	450 m	1000 m	60 m	130 m	120 m	250 m	380 m	790 m

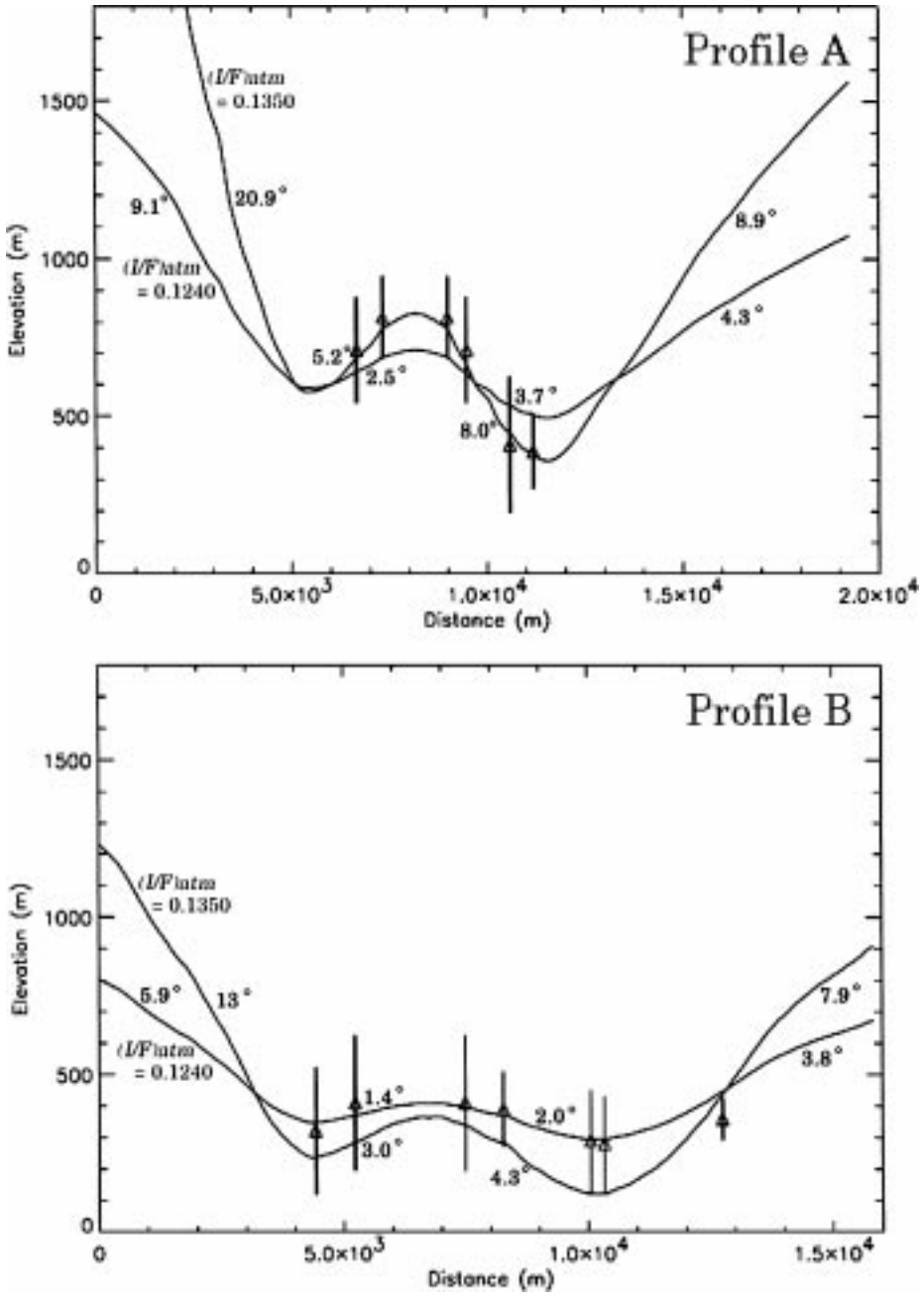

FIG. 3. Profiles A and B shown with extreme $\frac{I}{F}_{\text{atm}}$ values. Stereogrammetric elevations are shown (triangles) with error bars. Each profile is plotted from its northernmost point. Slopes are labeled. Given the extreme relief of the northern wall of Profile A when $\frac{I}{F}_{\text{atm}} = 0.135$, the lower $\frac{I}{F}_{\text{atm}}$ values are more reasonable.

layers are exposed in the bottom of the trough to the east (toward and beyond Profile B).

The southern (right-hand in Fig. 3) rim of the trough is lower than the northern (left-hand) side. In addition, south-facing (equatoward) slopes are steeper than north-facing (poleward) slopes. Troughs created by sublimation would form walls that are steeper on the side receiving more insolation (the northern or left-hand side), creating the observed rim height and slope asymmetry. This asymmetry has been observed in MOLA tracks over the northern polar troughs (Zuber *et al.* 1998) and is consistent with a model in which polar troughs are created by preferential sublimation of a low albedo area (Ivanov and Muhleman 2000). A lower sublimation rate on north-facing slopes and subsequent incomplete defrosting can cause slight accumulations (Howard *et al.* 1982a), obscuring layers and leading to gentler slopes.

We have used the assumption of horizontal layers to choose values for $\frac{I}{F}_{\text{horiz}}$ and to fit the profiles to stereogrammetric points. Once again we use the assumption of horizontal layers to

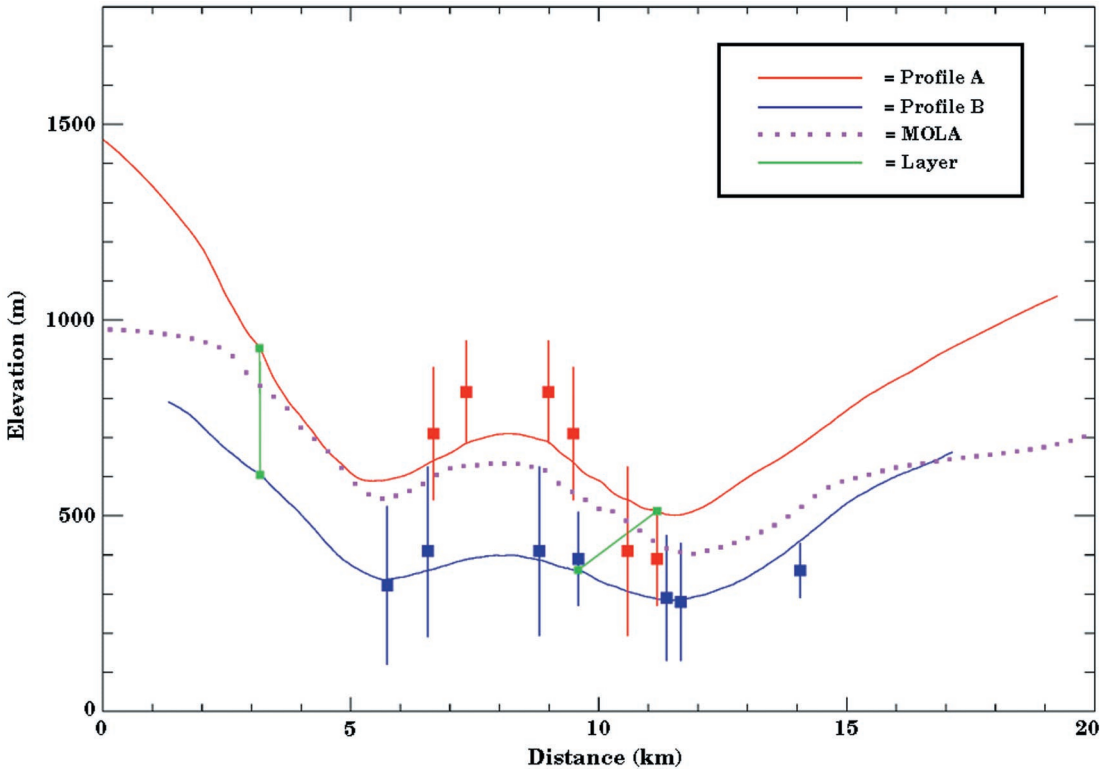

FIG. 4. Profiles A and B (with $\frac{I}{F}_{\text{atm}} = 0.124$) shown on the same graph with corresponding stereogrammetric elevations. The profiles have been shifted vertically to minimize the difference in elevation between layers crossing both profiles (shown in green). The MOLA track is shown, vertically shifted by 775 m.

position the profiles more accurately. As mentioned before, several layers cross both Profiles A and B. If these layers are horizontal then they must cross Profiles A and B at the same elevation. Both profiles can be shifted vertically as long as they remain within the stereogrammetric error bars.

Figure 4 shows Profiles A and B with their corresponding stereogrammetric points, vertically shifted so that coinciding layers are as close to horizontal as possible. The locations of two prominent layers are marked in green, showing where they cross each profile. The more northerly green marker bed is the same layer indicated by arrows in Fig. 1. The more southerly green marker bed has an elevation of 390 ± 120 m from the stereogrammetric measurements and it is used to constrain both photoclinometric profiles. Profiles A and B are aligned so the northernmost green layer is shown at the same horizontal position. Because the position of the MOLA track relative to the image (which has been controlled using *Viking* MDIM's) is somewhat ambiguous, it has been shifted so that it is aligned with both profiles.

If the layers are horizontal as assumed then the marker beds shown in green should be at the same elevation, but it is impossible to both make these layers exactly horizontal and keep the profiles within the stereogrammetric elevation error bars. According to the marker beds the dips are to the west at 0.93° and 0.43° for the north and south beds, respectively. Although small, these slopes are greater than the maximum 0.17° predicted, assuming the layers do not tilt with a relief greater than 10% of the height of the horizontal trough. This is exactly the situation that could not be detected by inspection of the images: one in which the layers and the trough tilt in the same direction. Although the tilting layers refute our assumption of level layers, we note that the actual dip is rather small and thus it will not significantly distort our results.

In addition to the drop in elevation, the relief between the two marker beds drops from ~425 m in Profile A to ~250 m in Profile B. The tilt and reduced relief can be explained by a decrease in layer thickness to the east, implying a corresponding decrease in net accumulation. The change in relief could also be caused by a net albedo change along the trough. The new MOLA profiles should allow for discrmination between these two cases.

It is unclear what caused the apparent eastward decrease in layer accumulation. Less material may have been deposited in this region. Alternatively, the sublimation rate may have been higher here than farther west. The resistance to erosion of the trough material may decrease with thickness, explaining the lower slopes and exposed deep layers in the eastern portion of the trough.

3.2. *MOLA Results*

In order to compare our photoclinometric profiles with new MOLA elevations, we searched for a MOLA profile crossing the

same trough as close as possible to the positions of Profiles A and B. The MOLA track from pass number 204 crosses the trough obliquely between Profiles A and B (see Fig. 2). Because the new Mars Global Surveyor latitudes and longitudes differ from those of the *Viking* MDIM's, the position of this MOLA track had to be plotted on top of the *Viking* images and manually shifted until surface features appeared to match. Because of this "eyeball method," positioning of the track may be in error up to 1 km (15 pixels in Fig. 2), but this approximate placement is adequate for qualitative comparison with our photoclinometric profiles.

MOLA elevations across the trough are shown in Fig. 4. Because the MOLA track crosses the trough obliquely, the elevations have been projected to a line parallel to Profile B for better comparison. The local topography from MOLA agrees well with the photoclinometric profiles with low atmospheric opacity. There are small discrepancies at both ends of the profile that are most likely caused by slight changes in albedo or atmospheric scattering that cannot be detected in the *Viking* image. However, the relief and slopes within the trough are remarkably similar to those produced by the photoclinometric profiles, indicating that the low $\frac{I}{F}_{\text{atm}}$ value (low opacity) is the most accurate.

Like the photoclinometric profiles, the MOLA track has been vertically shifted to fit between the stereogrammetric elevations. Because the *Mars Global Surveyor* spacecraft positioning is much more precise than that of the *Viking Orbiters*, measured elevations differ significantly from elevations from the *Viking* missions. We find the MOLA elevations are 775 m lower than *Viking* stereogrammetric elevations, well within the observed 1–2 km difference between MOLA elevations and the *Viking* DTM (Zeitler and Oberst 1999, Smith *et al.* 1998).

We attempted to find the elevations of individual layers on the MOLA track. Unfortunately, we could not obtain reliable layer elevations because of the uncertainty in positioning the MOLA track over a *Viking* image.

3.3. Layer Thicknesses

With the correct atmospheric contribution ($\frac{I}{F}_{\text{atm}}$) confirmed by MOLA, it is possible to accurately measure layer thicknesses. To achieve the best possible thickness estimates we measured layers on the summertime image 077B55, the clearest image of the three (see Fig. 1b). We assumed that the bright stripes are more level than the dark stripes, and as a result less ice has sublimated on the bright "stair-tops" relative to the dark, Sun-facing, steeper slopes (Howard *et al.* 1982a).

The resulting layers and their respective thicknesses in meters are shown in Fig. 5. At the location of Profile A, the layers on

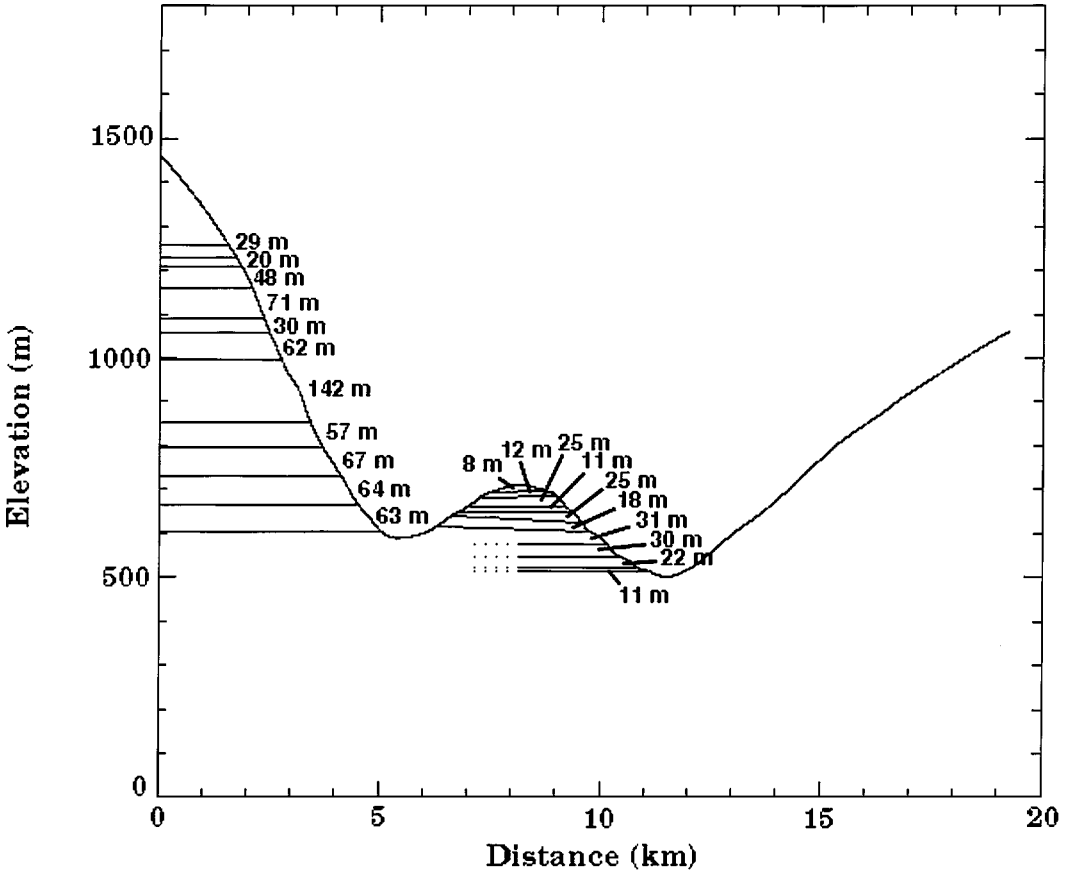

FIG. 5. Profile A ($\frac{I}{F}_{\text{atm}} = 0.124$) showing layers and layer thicknesses. Note how several more layers are visible on the midridge than on the north (left) wall. This difference is visible in Fig. 1b as well.

the northern wall have an average thickness and standard deviation of 59 ± 32 m and the layers on the midridge have an average thickness and standard deviation of 19 ± 8 m. The midridge layers almost certainly correspond to layers on the northern wall, although several smaller layers are exposed on the midridge that remain obscure on the northern wall. The midridge slopes are lower than the north wall slope; this gentler slope may expose thinner layers than the steeper north slope. Blasius *et al.* (1982a) also found thinner strata on gentler slopes and concluded that only the most shallow slopes provide useful stratigraphic information. One certain conclusion from this discrepancy is that smaller layers exist where they are not always apparent. Photoclinometry of this region with high-resolution MOC images will likely reveal much thinner layers than can be resolved in *Viking* images.

4. DISCUSSION

Because polar layer deposition is thought to be influenced by some cyclical climate change, it is important to calculate timescales for layer formation. Assuming that the northern wall includes obscured thinner layers that only appear on shallower slopes, the thinner layers on the midridge are used in this calculation. Given a deposition rate, it is possible to calculate a crude first-order estimate of layer formation time. This estimation does not account for change in deposition or sublimation rates that occur with changes in the amplitude of obliquity oscillations.

Herkenhoff and Plaut (1999) calculated a resurfacing rate of $1.165\,\text{mm year}^{-1}$. Assuming that this value represents a net rate of accumulation rather than erosion, each 19-m thick layer requires at most 16,000 years to form. This timescale is much shorter than the modeled 10^5- and 10^6-year obliquity variations (Ward 1974, 1979). Our calculation does not take into account factors such as ice compaction, but even if such factors doubled our estimate it would still fall short of the obliquity variation timescale. Furthermore, still thinner layers are present in the layered terrain that are below the resolution of *Viking* imagery (Edgett and Malin 2000). Such layers would take even less time to accumulate than our 10^4-year estimate. If our timescale is correct and the deposition rate is constant then the layers cannot be formed by any known orbital variation. However, it is possible that deposition only occurs during part of the obliquity cycle, resulting in a net accumulation of the observed thin layers. We agree with Thomas *et al.* (1992) in that without knowledge of which part of a climatic cycle layers form, our extrapolations are of "limited significance."

5. CONCLUSIONS

Photoclinometry creates reliable high-resolution topographic profiles when constrained by several absolute elevations. The assumptions that seasonal frost provides a uniform albedo covering, that the atmosphere can be approximated by a constant intensity value, and that layers are roughly horizontal have produced topographic profiles that qualitatively match a nearby MOLA profile. Creating photoclinometrically determined topographic profiles with MOC images constrained with MOLA elevations will be a powerful tool in studying the polar layered deposits at very high resolution.

The major findings of our study include:

(1) Our topographic profiles crossing a northern polar trough agree with the findings from both MOC and MOLA. In the northern polar region troughs are asymmetric with higher walls and steeper slopes facing the equator. The topographic expression of layers is very subtle relative to layers in the southern polar deposits. Northern polar deposits have a topography more subdued than that of the south at the scale of both individual layers and troughs. This difference in relief may be related to the age difference between the north and south polar layered terrains.

(2) Because of a decrease in relief from the western profile (Profile A) to the eastern profile (Profile B), we have found that the trough layers decrease in thickness to the east. This thinning of layers is accompanied by an eastward decrease in equatorward trough slopes, suggesting that erosional rates differ on layers of different thickness. Thus the resistance to erosion of the layered terrain may vary with layer thickness.

(3) Assuming that the net accumulation rate is the same as the recently calculated resurfacing rate (Herkenhoff and Plaut 1999), the average time required to form a layer is about 16,000 years, far shorter than any orbital oscillation. We conclude either that layers are formed during a limited part of the oscillation period or that the layers are formed by climate variations unrelated to known astronomical variations.

ACKNOWLEDGMENTS

We are grateful to Bruce Murray for advice and to Arden Albee for a detailed review of the manuscript. We also thank the reviewers (Stephen Clifford and anonymous) for their many helpful suggestions.

REFERENCES

Batson, R. M. 1987. Digital cartography of the planets: New methods, its status, and its future. *Photogramm. Eng. Remote Sens.* **53**, 1211–1218.

Bills, B. G. 1990. The rigid body obliquity history of Mars. *J. Geophys. Res.* **95**, 14,137–14,153.

Blasius, K. R., J. A. Cutts, and A. D. Howard 1982a. Topography and stratigraphy of martian polar layered deposits. *Icarus* **50**, 140–160.

Blasius, K. R., A. V. Vetrone, B. H. Lewis, and M. D. Martin 1982b. Viking Orbiter stereo imaging catalog. NASA Contractor Rept. 3501.

Carr, M. H. 1982. Periodic climate change on Mars: Review of evidence and effects on distribution of volatiles. *Icarus* **50**, 129–139.

Chapman, M. G. 1999. Elysium basin lava flow: New interpretations based on MOC data. *Lunar and Planetary Science 30*, Abstract 1279. Lunar and Planetary Institute, Houston. [CD-ROM]

Cutts, J. A., K. R. Blasius, G. A. Briggs, M. H. Carr, R. Greeley, and H. Masursky 1976. North polar region of Mars: Imaging results from Viking 2. *Science* **194**, 1329–1337.

Cutts, J. A., K. R. Blasius, and W. J. Roberts 1979. Evolution of martian polar landscapes: Interplay of long-term variations in perennial ice cover and dust storm intensity. *J. Geophys. Res.* **84**, 2975–2994.

Dzurisin, D., and K. R. Blasius 1975. Topography of the polar layered deposits of Mars. *J. Geophys. Res.* **80**, 3286–3306.

Edgett, K. S., and M. C. Malin 1999. MGS MOC the first year: Sedimentary materials and relationships. *Lunar and Planetary Science 30*, Abstract 1029, Lunar and Planetary Institute, Houston. [CD-ROM]

Edgett, K. S., and M. C. Malin 2000. Sedimentary bedding features of martian polar layered terrain. *Lunar and Planetary Science 31*, Abstract 1068. Lunar and Planetary Institute, Houston. [CD-ROM]

Edwards, K. 1987. Geometric processing of digital images of the planets. *Photogramm. Eng. Remote Sens.* **53**, 1219–1222.

Herkenhoff, K. E., and B. C. Murray 1990a. Color and albedo of the south polar layered deposits on Mars. *J. Geophys. Res.* **95**, 1343–1358.

Herkenhoff, K. E., and B. C. Murray 1990b. High resolution topography and albedo of the south polar layered deposits on Mars. *J. Geophys. Res.* **95**, 14,511–14,529.

Herkenhoff, K. E., and J. J. Plaut 1999. Ages and resurfacing rates of the polar layered deposits. In *The Fifth International Mars Science Conference*, Abstract 6065.

Howard, A. D., K. R. Blasius, and J. A. Cutts 1982b. Photoclinometric determination of the topography of the martian north polar cap. *Icarus* **50**, 245–258.

Howard, A. D., J. A. Cutts, and K. R. Blasius 1982a. Stratigraphic relationships within martian polar-cap deposits. *Icarus* **50**, 161–215.

Ivanov, A. B., and D. O. Muhleman 2000. The role of sublimation for the formation of the northern ice cap: Results from the Mars Orbiter Laser Altimeter. *Icarus* **144**, 436–448.

Malin, M. C. 1986. Density of martian north polar layered deposits: Implications for composition. *Geophys. Res. Lett.* **13**, 444–447.

Malin, M. C., and K. S. Edgett 1999. An emergent, new paradigm for Mars geology. In *The Fifth International Mars Science Conference*, Abstract 6027.

Murray, B. C., L. A. Soderblom, J. A. Cutts, R. P. Sharp, D. J. Milton, and R. B. Leighton 1972. Geological framework of the south polar region of Mars. *Icarus* **17**, 328–345.

Paige, D. A., and A. P. Ingersoll 1985. Annual heat balance of martian polar caps: Viking observations. *Science* **228**, 1160–1168.

Plaut, J. J., R. Kahn, E. A. Guinness, and R. E. Arvidson 1988. Accumulation of sedimentary debris in the south polar region of Mars and implications for climate history. *Icarus* **75**, 357–377.

Smith, D. E., M. T. Zuber, H. V. Frey, J. B. Garvin, J. W. Head, D. O. Muhleman, G. H. Pettengill, R. J. Phillips, S. C. Solomon, H. J. Zwally, and W. B. Banerdt 1998. Topography of the northern hemisphere of Mars from the Mars Orbiter Laser Altimeter. *Science* **279**, 1686–1692.

Squyres, S. W. 1979. The evolution of dust deposits in the martian north polar region. *Icarus* **40**, 244–261.

Thomas, P. C., and C. Weitz 1989. Dune sand materials and polar layered deposits on Mars. *Icarus* **81**, 185–215.

Thomas, P., K. Herkenhoff, A. Howard, B. Murray, and S. Squyres 1992. Polar deposits on Mars. In *Mars*, pp. 767–795. Univ. of Arizona Press, Tucson.

Toon, O. B., J. B. Pollack, W. Ward, J. A. Burns, and K. Bilski 1980. The astronomical theory of climatic change on Mars. *Icarus* **44**, 552–607.

Ward, W. R. 1974. Climatic variations on Mars. 1. Astronomical theory of insolation. *J. Geophys. Res.* **79**, 3375–3386.

Ward, W. R. 1979. Present obliquity oscillations of Mars: Fourth-order accuracy in orbital e and I. *J. Geophys. Res.* **84**, 237–241.

Zeitler, W., and J. Oberst 1999. The shape of Mars before Global Surveyor: Results from reanalysis of the Viking control point analysis. *J. Geophys. Res.* **104**, 14,051–14,063.

Zuber, M. T., D. E. Smith, S. C. Solomon, D. O. Muhleman, J. W. Head, J. B. Garvin, J. B. Abshire, and J. L. Bufton 1992. The Mars Observer Laser Altimeter investigation. *J. Geophys. Res.* **97**, 7781–7798.

Zuber, M. T., D. E. Smith, S. C. Solomon, J. B. Abshire, R. S. Afzal, O. Aharonson, K. Fishbaugh, P. G. Ford, H. V. Frey, J. B. Garvin, J. W. Head, A. B. Ivanov, C. L. Johnson, D. O. Muhleman, G. A. Neumann, G. H. Pettengill, R. J. Phillips, Z. L. Sun, H. J. Zwally, W. B. Banerdt, and T. C. Duxbury 1998. Observations of the north polar region of Mars from the Mars Orbiter Laser Altimeter. *Science* **282**, 2053–2060.